Published in final edited form as:
Neuroimage. 2014 April 15; 90: 235–245. doi:10.1016/j.neuroimage.2013.12.056.

In vivo Visuotopic Brain Mapping with Manganese-Enhanced MRI and Resting-State Functional Connectivity MRI

Kevin C. Chan[1,2,4,5,6,7,*,+], **Shu-Juan Fan**[1,2,+], **Russell W. Chan**[1,2], **Joe S. Cheng**[1,2], **Iris Y. Zhou**[1,2], and **Ed X. Wu**[1,2,3,**]

[1]Laboratory of Biomedical Imaging and Signal Processing, The University of Hong Kong, Pokfulam, Hong Kong SAR, China

[2]Department of Electrical and Electronic Engineering, The University of Hong Kong, Pokfulam, Hong Kong SAR, China

[3]Department of Anatomy, The University of Hong Kong, Pokfulam, Hong Kong SAR, China

[4]UPMC Eye Center, Ophthalmology and Visual Science Research Center, Department of Ophthalmology, School of Medicine, University of Pittsburgh, Pittsburgh, PA, USA

[5]Department of Bioengineering, Swanson School of Engineering, University of Pittsburgh, Pittsburgh, PA, USA

[6]Center for the Neural Basis of Cognition, University of Pittsburgh and Carnegie Mellon University, Pittsburgh, PA, USA

[7]Louis J. Fox Center for Vision Restoration, McGowan Institute for Regenerative Medicine, University of Pittsburgh, Pittsburgh, PA, USA

Abstract

The rodents are an increasingly important model for understanding the mechanisms of development, plasticity, functional specialization and disease in the visual system. However, limited tools have been available for assessing the structural and functional connectivity of the visual brain network globally, in vivo and longitudinally. There are also ongoing debates on whether functional brain connectivity directly reflects structural brain connectivity. In this study, we explored the feasibility of manganese-enhanced MRI (MEMRI) via 3 different routes of Mn^{2+} administration for visuotopic brain mapping and understanding of physiological transport in normal and visually deprived adult rats. In addition, resting-state functional connectivity MRI (RSfcMRI) was performed to evaluate the intrinsic functional network and structural-functional relationships in the corresponding anatomical visual brain connections traced by MEMRI. Upon intravitreal, subcortical, and intracortical Mn^{2+} injection, different topographic and layer-specific Mn enhancement patterns could be revealed in the visual cortex and subcortical visual nuclei along retinal, callosal, cortico-subcortical, transsynaptic and intracortical horizontal connections. Loss of visual input upon monocular enucleation to adult rats appeared to reduce interhemispheric

[*,**]Correspondence to: Kevin C. Chan, Ph.D., Departments of Ophthalmology and Bioengineering, University of Pittsburgh, Pittsburgh, PA, USA, Tel: (412) 624-1257 Fax: (412) 383-6799, chuenwing.chan@fulbrightmail.org Or Ed X. Wu, Ph.D., Laboratory of Biomedical Imaging and Signal Processing, Departments of Electrical and Electronic Engineering, Anatomy and Medicine, The University of Hong Kong, Hong Kong SAR, China, Tel: (852) 2819-9713 Fax: (852) 2819-9711, ewu@eee.hku.hk.
[+]Authors contributed equally to this manuscript.

polysynaptic Mn^{2+} transfer but not intra- or inter-hemispheric monosynaptic Mn^{2+} transport after Mn^{2+} injection into visual cortex. In normal adults, both structural and functional connectivity by MEMRI and RSfcMRI was stronger interhemispherically between bilateral primary/secondary visual cortex (V1/V2) transition zones (TZ) than between V1/V2 TZ and other cortical nuclei. Intrahemispherically, structural and functional connectivity was stronger between visual cortex and subcortical visual nuclei than between visual cortex and other subcortical nuclei. The current results demonstrated the sensitivity of MEMRI and RSfcMRI for assessing the neuroarchitecture, neurophysiology and structural-functional relationships of the visual brains in vivo. These may possess great potentials for effective monitoring and understanding of the basic anatomical and functional connections in the visual system during development, plasticity, disease, pharmacological interventions and genetic modifications in future studies.

Keywords

Manganese-enhanced MRI; resting-state functional connectivity; retinal projection; cortico-cortical connection; cortico-subcortical connection; visuotopic brain mapping

INTRODUCTION

The rodents are an excellent model for understanding the mechanisms of development, plasticity, functional specialization and disease in the visual system (Chan et al., 2010a; Chan et al., 2008b; Chan et al., 2009a; Chan et al., 2009b; Chan et al., 2010b; Greenberg et al., 2008; Lau et al., 2011a; Lau et al., 2011b; Marshel et al., 2011; Millecamps and Julien, 2013; Wang et al., 2011; Zhang et al., 2012; Zhou et al., 2011; Zoccolan et al., 2009). In normal adult rodents, more than 90% of axons of retinal ganglion cells in the eye project contralaterally to the superior colliculus (SC) and lateral geniculate nucleus (LGN) (Kondo et al., 1993; Liu et al., 2011). The rodent retina also projects more axons to the SC than LGN as opposed to human (Dreher et al., 1985). On the other hand, the superficial gray layer of the SC receives about 90% of its excitatory input from the retina (Lund and Lund, 1971) and the remainder 10% from the visual cortex (Harvey and Worthington, 1990), whereas only 5–10% of relay cells in dorsal LGN receive retino-thalamic feedforward projections from the retina, and over 90% of relay cells in dorsal LGN receive corticothalamic feedback projections from the ipsilateral primary visual cortex (V1) (Jurgens et al., 2012; Sanderson et al., 1991; Sherman and Guillery, 2002). The visual cortex receives subcortico-cortical and cortico-cortical projections and sends out cortico-cortical and cortico-subcortical projections intra- and inter-hemispherically in a layer-specific manner (Alonso and Swadlow, 2005; Coogan and Burkhalter, 1993; Martinez-Garcia et al., 1994). In particular, callosal cells are densely located in the transition zone of the primary/secondary visual cortex (V1/V2) (Olavarria and Van Sluyters, 1983), and project axons to a narrow area in the contralateral hemisphere (Innocenti et al., 1995; Mizuno et al., 2007). The topographic layout of the retina is also represented in the SC, LGN, visual callosal fibers and each cortical visual area (Coleman et al., 2009; Cusick and Lund, 1981; Montero, 1993; Olavarria et al., 2008). To date, limited tools have been available for in vivo, high-resolution mapping of neuroarchitecture in the visual brains globally and longitudinally (Antonini et al., 1999; Greenberg et al., 2008; Wang et al., 2007). There are also ongoing debates among neuroscientists on whether functional brain connectivity directly reflects structural brain connectivity (Damoiseaux and Greicius, 2009; Dawson et al., 2013; Greicius et al., 2009; Hermundstad et al., 2013; Honey et al., 2009). Mn^{2+} has been increasingly used as a positive T1-weighted contrast agent for in vivo neuronal tract tracing (Canals et al., 2008; Chan et al., 2011a; Chan et al., 2011b; Chan et al., 2008c; Chan et al., 2007; Chan et al., 2011c; Liang et al., 2011; Pautler, 2004; Pautler et al., 1998; Soria et al., 2008; Tucciarone et al., 2009), detection of neuroanatomy, pathophysiology and neuropharmacological changes

(Aoki et al., 2004; Chan et al., 2008a; Jelescu et al., 2013; Silva et al., 2008; Yang et al., 2008; Yang and Wu, 2008) and functional brain mapping at lamina levels (Bissig and Berkowitz, 2011; Chan et al., 2011c; Lin and Koretsky, 1997; Watanabe et al., 2004; Yu et al., 2005). However, transsynaptic illumination of the visual cortex via intravitreal Mn^{2+} injection has been shown to be of limited sensitivity (Lindsey et al., 2007). There is also limited information about the mechanisms of physiological transport within cortico-cortical and cortico-subcortical networks in the visual brain. In this study, we explored the capability of Mn-enhanced MRI (MEMRI) via 3 different routes of Mn^{2+} administration for in vivo assessments of retinal, callosal, transsynaptic, corticothalamic, corticocollicular and intracortical horizontal connections in normal and visually deprived adult rat brains. In addition, resting-state functional connectivity MRI (RSfcMRI) using blood oxygen level dependent contrast was performed to evaluate the intrinsic functional networks in the corresponding anatomical visual brain connections traced by MEMRI, and to determine the structural-functional relationships within rat visual brain network. Our results demonstrated the sensitivity of MEMRI and RSfcMRI for assessing the neuroarchitecture, neurophysiology and structural-functional relationships of the visual brains in vivo, and may possess great potentials for studying the basic anatomical and functional connections in the visual system during development, plasticity, disease, pharmacological interventions and genetic modifications.

MATERIALS AND METHODS

Animal Preparation

Adult Sprague-Dawley rats (N=46; 200–250 g; Charles River Lab, USA) were divided into 4 groups. In Group 1 (n=4), a fractionated dose of Mn^{2+} at 3μL and 50mM each was injected intravitreally into the left eye every day for a total of 3 days; In Group 2 (n=6), Mn^{2+} was injected unilaterally into the left LGN at 30nL and 100mM; In Group 3 (n=29), Mn^{2+} was injected intracortically to the primary/secondary visual cortex (V1/V2) transition zone (TZ) of the right hemisphere at 100nL and 100mM (Group 3a; n=7) or 500mM (Group 3b; n=12; Group 3c; n=10) at about 6.5 mm posterior and 5.5 mm lateral to Bregma. In addition, 5 rats in Group 3c received left eye enucleation at 1 week before Mn^{2+} injection to eliminate visual input from left eye to the visual cortex. For Group 1, MEMRI was performed before, and at 1, 2 and 3 days after initial Mn^{2+} intravitreal injection. For Groups 2 and 3a, MEMRI was performed at 1 hour, 8 hours and 1 day after Mn^{2+} administration. For Group 3b, MEMRI was performed 24 hours before (n=12), and at 8 hours (n=5), 24 hours (n=12) and 48 hours (n=3) after Mn^{2+} injection. For Group 3c, MEMRI was performed at 8 and 24 hours after Mn^{2+} administration. In addition, 7 rats were untreated and underwent RSfcMRI (Group 4a: n=4; Group 4b: n=3). Three days after RSfcMRI, Mn^{2+} (100nL, 100mM) was injected into the visual cortex of 3 rats (Group 4b). MEMRI was acquired 24 hours after injection.

MRI Protocols

All MRI measurements were acquired utilizing a 7 T Bruker scanner with a maximum gradient of 360 mT/m (70/16 PharmaScan, Bruker Biospin GmbH, Germany), a 72 mm birdcage transmit-only RF coil and an actively decoupled receive-only quadrature surface coil. Under inhaled isoflurane anaesthesia (3% induction and 1.2%–1.5% maintenance), animals were kept warm under circulating water at 37°C. Continuous monitoring of the respiration rate, heart rate, oxygenation saturation and rectal temperature was performed and maintained within normal physiological ranges. Scout T2-weighted (T2W) images were first acquired in three planes with a rapid acquisition with relaxation enhancement (RARE) pulse sequence to position the subsequent MR images along standard anatomical orientations in a reproducible manner. For Groups 1 to 3a, 2D T1-weighted (T1W) spin-echo RARE pulse

sequence was acquired with repetition time/echo time (TR/TE) = 475/8.8 ms, field of view/slice thickness (FOV/th) = 32×32 mm^2/0.8 mm, matrix resolution (MTX) = 256×256, acquired resolution = 125×125 μm^2, number of slices = 10, RARE factor = 4 and acquisition time = 15 min. For Groups 3b, 3c and 4b, modified driven equilibrium Fourier transform (MDEFT) imaging sequence were employed for characterizing Mn^{2+} enhancement with TR = 4000 ms, echo TR/TE = 12/4 ms, inversion time (TI) = 1100 ms, number of segments = 4, number of averages = 8, FOV = 32 × 32 mm^2, MTX = 256 × 256 (Groups 3b and 3c) or 64×64 (Group 4b), slice thickness = 0.5 mm (Groups 3b and 3c) or 1 mm (Group 4b), number of slices = 28 (Groups 3b and 3c) and 16 (Group 4b) and acquisition time = 60 min. For RSfcMRI, a single-shot gradient-echo echo-planar-imaging (EPI) sequence was used with TR/TE = 1000/18ms, FOV = 32×32mm^2, MTX = 64×64, ten 0.8-mm (Group 4a) or 1-mm (Group 4b) thick contiguous slices and 420 (Group 4a) or 400 (Group 4b) repetitions. It resulted in about 7 minutes of scan time for each RSfcMRI dataset and 3–6 datasets were acquired for each animal. RARE T2W images were acquired under the same spatial dimensions with TR/TE = 4200/36 ms, 256 × 256 matrix as an anatomic reference for MDEFT and EPI data.

Data Analysis

For Groups 1 to 3a, T1W signal intensities (SI) in the SC, LGN, V1, and V1/V2 transition zone of each hemisphere, and in the splenium of corpus callosum (CC) were measured using ImageJ v1.43u (Wayne Rasband, NIH, USA) based on the anatomical landmarks in rat brain atlas (Paxinos and Watson, 2007a), and were normalized to the surrounding muscles. Mn^{2+} enhancement was quantified by calculating the ratio between left and right visual components in Groups 1 and 2, and the rate of signal increase at Hour 8 and Day 1 compared to Hour 1 in Group 3a. Values at each time point were compared to the first time point using two-tailed paired t-tests.

To depict interhemispheric Mn^{2+} transport along the corpus callosum, MDEFT images from normal animals were normalized by background noise level and reconstructed three-dimensionally using AMIRA 5.2.2 (Visage Imaging Inc.) in Group 3b. For semi-quantitative analysis of the left contralateral enhancement patterns at both 8 hrs and 24 hrs, regions of interest (ROIs) were manually delineated in five consecutive MDEFT slices containing most prominent left hemisphere enhancement near the V1/V2 transition zone by referencing to a rat brain atlas (Paxinos and Watson, 2005). ROIs were defined as a stripe along the cortical depth direction over the most enhanced pixels or medial-laterally along the cortical surface direction. Signal intensity profiles of these ROIs were plotted using ImageJ, averaged among five slices in each animal and normalized to the right parietal cortex. T1W SI of the left V1/V2 transition zone, corpus callosum and right LGN were also normalized by those of the right cortex for statistical comparisons between normal and monocularly enucleated rats. Normalized and mean signal intensities of these ROIs were compared using one-way analysis of variance (ANOVA) with Bonferroni's multiple comparison tests. Data are shown as mean ± standard deviation unless otherwise specified. Results were considered significant when $p<0.05$.

For each RSfcMRI dataset in Group 4a, all images were first corrected for slice timing differences using SPM5 and then realigned to the mean image of the series using 2D rigid-body transformation with AIR v5.2.5 (Roger Woods, UCLA, USA). A voxel-wise linear detrending with least-square estimation was performed temporally to eliminate the baseline drift caused by physiological noises and system instability. In-plane smoothing was done using a Gaussian kernel with full width at half maximum of 1 × 1 mm^2. Finally, a temporal band-pass filter (0.005–0.1Hz) was applied to all voxels to extract the low frequency fluctuations. Seed-based analysis was performed on the following functional brain areas, including monocular V1 (V1M), binocular V1 (V1B), V1/V2 transition zone (V1/V2),

medial secondary visual cortex (V2M), lateral secondary visual cortex (V2L), superficial layers of SC (sSC), deep layers of SC (dSC), dorsal LGN (dLGN), ventral LGN (vLGN), primary sensorimotor cortex (S1) and auditory cortex (AC). A 4-voxel region centered at each functional area as defined in the rat brain atlas (Paxinos and Watson, 2007b) was chosen as the seed. For each functional brain area, two seeds located symmetrically in the left and right hemispheres were used respectively. Cross correlation coefficient (ccc) was calculated between average time course of the seed and every other voxel time course.

For comparisons between RSfcMRI and MEMRI in the same animals in Group 4b, all MEMRI images were co-registered using T2-weighted images as a reference. A 4×4 seed voxel was placed near the injection site and its signal intensity was used to normalize the T1-weighted MDEFT images. An ROI was defined to cover the contralateral left visual cortex as in Fig. 7 based on rat brain atlas (Paxinos and Watson, 2007a). Signal intensities of the voxels within the ROI were extracted for quantitation in the visual cortex. All RSfcMRI data were compensated for slice timing, detrended, realigned as well as temporally low-pass filtered to obtain low frequency fluctuations as in Group 4a. Subsequently, inter-animal co-registration was performed using their respective T2-weighted image as a reference. Correlation coefficient maps were obtained using seed based analysis with a 4×4 seed voxel on the V1/V2 border and the somatosensory cortex each. The correlation coefficients in the ROI were extracted for quantitation in the visual cortex, and were plotted against normalized MEMRI signal intensities in the same ROI in a voxel-by-voxel basis.

RESULTS

In vivo MEMRI for Visuotopic Brain Mapping

Intravitreal, fractionated MEMRI of Retinal and Transsynaptic Connections—In normal adult brains in Group 1, fractionated, intravitreal Mn^{2+} injection resulted in significant Mn enhancements in contralateral SC (open arrows) and LGN (arrowheads) by 45–60% at 1–3 days after initial Mn^{2+} injection, and in contralateral V1 (closed arrows) by about 10% at 2–3 days after initial Mn^{2+} injection (Fig. 1a). Contralateral SC appeared to enhance slightly more than contralateral LGN at all times after initial Mn^{2+} injection.

Subcortical, single-dose MEMRI of Thalamo-cortical Connections—Direct, single-dose Mn^{2+} injection to LGN (arrowheads) in Group 2 resulted in Mn enhancement by 13–21% in ipsilateral V1 (arrows), and 8–11% in ipsilateral SC at 8–24 hours after Mn^{2+} injection (Fig. 1b). Mn enhancement in the LGN remained significantly higher than ipsilateral V1 and SC throughout the experimental period.

Intracortical, single-dose MEMRI of Callosal, Cortico-subcortical and Intracortical Horizontal Connections—Intracortical, single-dose Mn^{2+} injection to the visual cortex in Group 3a resulted in Mn enhancement by 17–25% in contralateral V1/V2 transition zone (closed arrows), 32–34% in corpus callosum (open arrows), 53–65% in ipsilateral dorsal LGN (dashed arrows) and 15–26% in ipsilateral SC (arrowheads) at Hours 8–24 using RARE T1W sequence (Fig. 1c). Notably, layer-specific enhancement could be observed across the contralateral V1/V2 transition zone (Figs. 1c and 2). Some intracortical horizontal connections were also observed as a bi-laminar stripe in the ipsilateral right hemisphere (Fig. 2). When comparing between different routes of Mn^{2+} injection, topographic Mn enhancement could be differentiated, with intravitreal Mn^{2+} injection and subcortical Mn^{2+} injection enhancing more medially at the visual cortex subdivisions V1M and V1B compared to intracortical Mn^{2+} injection, which enhanced predominantly near the V1/V2 border (Fig. 2). Intracortical Mn^{2+} injection also showed more localized Mn

enhancement at dorsal LGN via cortico-subcortical Mn^{2+} transport than intravitreal Mn^{2+} injection via retino-thalamic Mn^{2+} transport (Figs. 1 and 3).

To investigate the interhemispheric connections more comprehensively across different MRI parametric settings, we employed MDEFT sequence at a longer acquisition time, thinner slices, and a higher Mn^{2+} dosage before, and at 8 hours, 1 day and 2 days after Mn^{2+} injection to right visual cortex in Group 3b (Figs. 3 to 5). Before $MnCl_2$ injection, the corpus callosum consistently showed lower signal intensity than the surrounding white matter. At 8 hours after injection, the corpus callosum was significantly enhanced and was seen brighter than the surrounding white matter. At 1 day and later after injection, the corpus callosum gradually became less distinguished from the surrounding white matter (Figs. 3A and 3B, arrowheads). In the left hemisphere contralateral to the injection site, significant Mn enhancement was observed at the V1/V2 transition zone at all three time points after injection in all rats (Fig. 3A, right panel, short arrows). Such enhancement exhibited first as a narrow stripe at Hour 8. It then expanded medial-laterally with increased signal intensity and exhibited a prominent bi-laminar pattern at Hour 24 (Fig. 3A, right panel, long arrows). At Hour 48, it further expanded medial-laterally with decreased signal intensity. The three-dimensionally reconstructed MDEFT images clearly depicted the Mn^{2+} transport pathway via corpus callosum (Figs. 4B and 4E, white arrowheads). The Mn^{2+} transport pathway originated from the injected right hemisphere as a thick band, first going rostrally along the visual callosal projection in the ipsilateral hemisphere, then caudally after crossing the midline (Fig. 4B, inset) and finally reaching V1/V2 border (Fig. 4B, red arrowhead). Such enhancement pattern maintained at 24 hrs after injection (Figs. 4D to 4F). Temporally, the enhancement in the left V1/V2 transition zone preferably spread more medial-laterally (Figs. 4B & 4E, red arrowhead) than anterior-posteriorly (Figs. 4C & 4F) while the ipsilateral enhancement in the right hemisphere exhibited a relatively isotropic expansion, but with slightly faster layer-specific Mn^{2+} transport along intracortical horizontal connections.

The stripe-like bi-laminar Mn^{2+} enhancement pattern in the contralateral left V1/V2 transition zone was analyzed semi-quantitatively in five animals at 8 hrs and 24 hrs after injection in normal adult rats (Fig. 3B and Fig. 5) by plotting the pixel-by-pixel signal intensity along cortical depth direction (Fig. 5A) or medial-laterally along the cortical surface (Fig. 5B). The cortex was divided into six layers based on published MRI and histological results (Bissig and Berkowitz, 2009; Failor et al., 2010). The enhancement peaked in layers II/III and V at both Hours 8 and 24, with layer IV being more distinguishable from surrounding layers at Hour 24. Medial-laterally, Mn enhancement was confined within 1 mm from the V1/V2 border at Hour 8, peaked at V1/V2 border, and gradually decreased from the V1/V2 border in similar spatial profiles bilaterally. At Hour 24 such enhancement increased further and expanded beyond 1 mm from the V1/V2 border medial-laterally.

Intra- and inter-hemispheric Mn^{2+} transport between normal and monocularly enucleated rats—Comparing the cortico-cortical and cortico-subcortical Mn^{2+} transport between normal (Group 3b) and monocularly enucleated rats (Group 3c), as shown in Fig. 5C, no statistical difference was observed in corpus callosum and right LGN enhancement between two groups after intracortical Mn^{2+} injection to right visual cortex, while the left V1/V2 transition zone was significantly less enhanced in the monocularly enucleated rats than normal rats by about 18.5%. Figs. 5A and 5B showed a global decrease in Mn^{2+} enhancement at the contralateral left V1/V2 transition zone both across cortical depth and along medial-lateral directions in the monocularly enucleated rats compared to normal rats.

Resting state functional connectivity MRI of visual brain network

In the cross-correlation coefficient (ccc) map of spontaneous low frequency fluctuations between different brain regions among Group 4a animals in Fig. 6, intrahemispheric cortical connectivity [e.g. corticocortical (LvsL) network] appeared to be in general stronger than interhemispheric cortical connectivity [e.g. corticocortical (LvsR) network] ($p<0.05$), whereas corticocortical connectivity appeared to be in general stronger than cortico-subcortical connectivity intra- and inter-hemispherically ($p<0.05$). Comparing among interhemispheric cortico-cortical network, V1/V2 transition zone in one hemisphere possessed the highest mean correlation coefficient with the contralateral V1/V2 transition zone relative to other visual cortical nuclei measured in the contralateral hemisphere. At the same time, high functional connectivity was observed bilaterally between homotopic visual cortical regions where there was little or no direct structural connectivity as shown in MEMRI. Comparing among cortico-subcortical network, the functional connectivity between visual cortex and superficial layers of SC was apparently stronger than the less direct visual anatomical network in visual cortex vs deep layers of SC ($p<0.05$). The primary somatosensory cortex (S1) appeared to have a stronger correlation with the visual brain network compared to the primary auditory cortex (Aud1) in the same hemisphere ($p<0.05$). In Fig. 7, voxel-by-voxel comparisons between RSfcMRI and MEMRI in the left visual cortex of rats from Group 4b, indicated the strong positive correlation between functional connectivity using right V1/V2 as a seed voxel and the normalized signal intensities in MEMRI upon Mn injection into right visual cortex.

DISCUSSION

The results of this study showed that MEMRI and RSfcMRI were sensitive for assessing the neuroarchitecture, neurophysiology and structural-functional relationships of the visual brains in vivo. MEMRI allowed layer-specific and topographic brain mapping of retinal, callosal, cortico-subcortical, transsynaptic and intracortical horizontal connections in the visual system. Loss of visual input upon left eye enucleation appeared to reduce interhemispheric polysynaptic Mn^{2+} transfer but not intra- or inter-hemispheric monosynaptic Mn^{2+} transport. Strengths of intra- and inter-hemispheric resting-state functional connectivity appeared to couple with structural connectivity revealed by MEMRI in the visual brain network. These structural and functional visuotopic brain mapping techniques may help determine the developmental, pathophysiological and neuroplastic mechanisms in the developing and impaired living visual brains globally and longitudinally in a single setting in future studies.

In vivo MEMRI of Retinal, Subcortico-cortical and Transsynaptic Connections

Upon intravitreal Mn^{2+} injection, Mn^{2+} ions were taken up by the retinal ganglion cells, underwent anterograde axonal transport along the optic nerve and tract, and accumulated at the axonal terminals in the contralateral SC and LGN of the adult rat brain (Pautler et al., 1998; Watanabe et al., 2004). In the current study, contralateral SC appeared to enhance slightly more than contralateral LGN at all times after initial Mn^{2+} injection. This apparently agreed with the fact that axons from retina project to the contralateral SC more than the LGN in rodents (Dreher et al., 1985; Liu et al., 2011). Although transneuronal Mn^{2+} transport has been shown to occur in the brain (Pautler, 2004), transsynaptic illumination of the visual cortex via intravitreal Mn^{2+} injection has been difficult (Lindsey et al., 2007). Olson et al recently demonstrated that the degree of Mn enhancement in the visual pathway is determined by the duration of availability of Mn^{2+} from the vitreous body but not the injected dose (Olsen et al., 2010). Given the rapid clearance of Mn from the vitreous body (Olsen et al., 2010), this study evaluated the Mn enhancement in V1 upon (i) fractionated intravitreal injections or (ii) direct, single-dose injection to the LGN. As shown in Fig. 1,

daily, fractionated intravitreal injection resulted in about 10% of Mn enhancement in contralateral V1 starting at Day 2, whereas direct, single-dose injection into the LGN resulted in more than 10% of enhancement in the ipsilateral V1 as early as at 8 hours after injection. The results of these experiments demonstrated the feasibility of MEMRI to evaluate both monosynaptic and polysynaptic anterograde transport in the retinal projections longitudinally with improved sensitivity upon prolonged Mn input to localized visual components. To minimize invasiveness from multiple needle insertions, future studies may use controlled release of Mn^{2+} instead of multiple doses of daily intravitreal Mn^{2+} injections for sustained Mn^{2+} retinal input and Mn^{2+} accumulation at target visual nuclei (Morch et al., 2012). Future studies may also use the less toxic Mn-chelates such as Mn-DPDP for visuotopic brain mapping (Olsen et al., 2008).

In vivo MEMRI of Cortico-cortical Connections

Upon intracortical Mn^{2+} injection, MEMRI characterized spatiotemporally the layer-specific interhemispheric Mn^{2+} transport via the splenium of corpus callosum in the rodent visual brain in vivo. After Mn^{2+} ions were administered into the right V1/V2 border, they were transcallosally transported to the left hemisphere, and were collectively accumulated in the V1/V2 transition zone. The most prominent enhancement was observed in layers II/III and V, which was in agreement with histological tracing studies (Alonso and Swadlow, 2005; Coogan and Burkhalter, 1993; Dreher et al., 1990; Inoue et al., 2011; Martinez-Garcia et al., 1994). Temporally, Mn enhancement was initially confined within approximately 1 mm from the left V1/V2 border at Hour 8. It then enhanced further and spread more medial-laterally from the V1/V2 border in similar spatial profiles as in Hour 8. The laminar-specific enhancement in the right ipsilateral cortex lateral and medial to injection site in Figs. 2 and 3 also suggested that bilateral Mn transport occurred along intracortical horizontal connections faster than the general diffusion of Mn from the injection site. The above results indicated that MEMRI can serve as an effective tool for tracing anatomical intra- and inter-hemispheric connections similar to histological tracing techniques but in the whole living visual brains without depth limitations. Future studies may also use MEMRI at a lower Mn^{2+} injection dose and volume to trace localized axonal projections in a more precise manner.

In vivo MEMRI of Cortico-subcortical Connections

The dorsal LGN (dLGN) serves as the primary conduit of retinal information to visual cortex in the mammal brains. In addition to retinal input, dLGN receives a large feedback corticothalamic projection locally from layer VI of the visual cortex, which provides a powerful substrate for modulating retinogeniculate signal transmission (Jurgens et al., 2012; Sherman and Guillery, 2002). In this study, upon intracortical Mn^{2+} injection the ipsilateral LGN appeared to enhance at the highest rate compared to other measured visual components at Hour 8, possibility because of the short distance and high density of cortico-geniculate connections in the visual brain (Jurgens et al., 2012; Sanderson et al., 1991; Sherman and Guillery, 2002). The Mn accumulation appeared to slow down from Hours 8 to 24 in the ipsilateral LGN and the corpus callosum. On the other hand, the contralateral V1/V2 and ipsilateral SC, whose connections to the injection site at ipsilateral V1/V2 were more distant than ipsilateral LGN and SC, continued to enhance steadily at Hour 24.

Mn^{2+} has been estimated to be taken up by the retinal ganglion cells and subsequently transported along retinocollicular projections at a rate of about 2.8 mm/h in rats (Watanabe et al., 2004). In this study, the interhemispheric distance between the injection site in the right hemisphere and the left V1/V2 transition zone was around 11 mm (Paxinos and Watson, 2005). Therefore, one might expect that Mn^{2+} might reach the contralateral V1/V2 transition zone starting at about Hour 4, and even earlier for subcortical visual nuclei

assuming similar transport rate as in the retinocollicular pathway. Mn enhancements at both Hours 8 and 24 might therefore reflect the integrity of neuronal Mn^{2+} uptake in right Mn^{2+} injected hemisphere, the transcallosal or cortico-subcortical Mn^{2+} transport and the activity-driven Mn^{2+} accumulation in the visual target nuclei over time. Axonal transport of Mn^{2+} can be anterograde (Bilgen, 2006; Pautler et al., 1998), retrograde (Matsuda et al., 2010) or mixed (Pautler et al., 2003). The callosal cells in the two hemispheres could be interlinked by independent axonal projections to the contralateral hemisphere (Innocenti, 1986; Innocenti et al., 1995; Karayannis et al., 2007). The SC and LGN also send and receive axonal projections to and from the visual cortex. Although it is not clear in this study whether both active anterograde and retrograde Mn^{2+} transport was involved in the Mn enhancement, recent studies estimated that the bulk rate of active anterograde transport along the rat visual pathway was approximately 2–3 times faster than active retrograde transport (Abbott et al., 2013). It has also been shown ex vivo that injection of retrograde tracer horseradish peroxide into V1/V2 transition zone would result in more widespread labeling of neurons in primary and secondary cortices in the contralateral hemisphere (Miller and Vogt, 1984b), rather than the current MEMRI observation of localized V1/V2 enhancement in the contralateral hemisphere. It is therefore speculated that the current MEMRI observations of enhanced cortico-cortical and cortico-subcortical connections within the experimental period reflected axonal projections predominantly undergoing active anterograde transport. Future studies may employ high temporal resolution MEMRI and specific anterograde or retrograde axonal transport inhibitors to determine the contribution from active anterograde and retrograde transport by callosal cells, relay cells, excitatory pyramids or inhibitory interneurons in the visual brain.

Intra- and inter-hemispheric Mn^{2+} transfer upon total loss of monocular visual input—Upon neonatal binocular enucleation, our recent study using unilateral intracortical Mn^{2+} injection to the visual cortex of adult rats enhanced a larger projection volume by about 74% in the V1/V2 transition zone of the contralateral hemisphere compared to normal rats, suggestive of an adaptive change in interhemispheric connections and spatial specificity in the visual cortex upon early blindness (Chan et al., 2012). In the current study, upon left eye enucleation to adult rats, no apparent increase in the projection volume was observed in MEMRI at the V1/V2 transition zone (Fig. 5). This appeared to be consistent with previous histological studies showing age-dependent neuroplastic enlargement of the visual callosal projection to the primary visual cortex contralateral to the remaining eye in monocularly enucleated rats (Pietrasanta et al., 2012; Wree et al., 1986), whereby enucleation performed later than postnatal day 10 could not alter the overall spatial configuration of callosal neurons along the V1/V2 border (Rothblat and Hayes, 1982) and thus the similar Mn-projected volume at V1/V2 in normal and ME rats in this study. At the same time, left eye enucleation to adult rats for 1 week in this study could result in the contralateral right visual cortex largely deprived of visual input with little to no functional recovery (Van Brussel et al., 2011). Structural plasticity might also occur in the visual cortex upon visual input loss (Pan et al., 2007). In a previous study upon complete retinal lesion in mice, a lasting reduction in the number of inhibitory cell spines and boutons which form glutamatergic synapses was observed in the visual cortex, presumably causing a loss of glutamatergic input to these cells in conjunction with a decrease in the cells' synaptic output (Keck et al., 2011). Mn-enhanced MRI intensity has been suggested to reflect glutamate and calcium activities in the brain (Lin and Koretsky, 1997). As shown in Fig. 5C, the interhemispheric Mn^{2+} transfer dropped by 18.5% at the left V1/V2 transition zone upon right visual cortex Mn^{2+} injection compared to normal rats. However, no significant difference in Mn^{2+} enhancement in the corpus callosum or LGN through direct anterograde or retrograde axonal transfer was observed. These results echoed with the findings by Bearer et al and supported that electrical activity may not be necessary for uptake and monosynaptic transport of Mn^{2+},

but was required for its multiple synaptic transmission (Bearer et al., 2007). In summary, this study for the first time demonstrated that MEMRI is capable of tracing layer-specific transcallosal connectivity of visual cortex and is potentially sensitive to activity modulation. Combined with newly available Mn^{2+} administration methods, including infusion with engineered mini-pumps, MEMRI will enable both long-term and short-term in vivo studies with negligible toxicity, and may expediate the research into cortical development and plasticity.

RSfcMRI of Cortico-cortical and Cortico-subcortical Connections

In this study, the spontaneous low frequency fluctuations between different brain regions was assessed between specific visual brain regions (e.g. V1M, V1B, V2M, V2L, V1/V2, sSC, dSC, dLGN, vLGN) and between visual nuclei and somatosensory and auditory cortical nuclei in more detail than previous rodent RSfcMRI studies (Hutchison et al., 2010; Pawela et al., 2008). As seen in Fig. 6, intrahemispheric cortical functional connectivity was in general stronger than interhemispheric cortical functional connectivity, whereas corticocortical functional connectivity appeared to be stronger than cortico-subcortical functional connectivity both intra- and inter-hemispherically. Specifically, it is interesting to note that V1/V2 transition zone in one hemisphere was found to possess the highest mean correlation coefficient with the contralateral V1/V2 transition zone compared to other cortical nuclei measured in the contralateral hemisphere. This appeared to be consistent with our MEMRI observations in Figs. 1–5, showing more Mn enhancement in the anatomical transcallosal connections to contralateral V1/V2 transition zone upon intracortical Mn^{2+} injection to ipsilateral V1/V2 transition zone. Comparing within cortico-subcortical network, those with more direct anatomical visual connections traced by MEMRI (e.g. visual cortex vs superficial layers of SC) also showed stronger functional connectivity than the less direct anatomical network (e.g. visual cortex vs deep layers of SC). These observations appeared to support the recent hypotheses on a strong relationship between structural and functional connectivity across intra- and inter-hemispheric brain regions (Zhou et al., 2013; Zhou et al., 2012). Mn transport can be activity-driven and occurs via both axonal connections and neuron synapse terminals. The results in Fig. 7 showed a strong positive correlation between normalized signal intensities in MEMRI and correlation coefficients in RSfcMRI in the visual cortex upon Mn injection and seed voxel placement to contralateral visual cortex respectively. These results suggested a tight coupling between structural and functional connections in the bilateral visual cortex. Primary somatosensory cortex (S1) appeared to have a stronger correlation with the visual network compared to primary auditory cortex (Aud1) in RSfcMRI in Fig. 6. Whether such functional connectivity difference was related to structural interconnections among visual, somatosensory and auditory cortices (Miller and Vogt, 1984a; Van Brussel et al., 2011) remained to be elucidated. Recent evidence from human brain RSfcMRI studies suggested that blind subjects exhibited reduced functional connectivity in the bilateral visual cortex, and between visual cortex and sensorimotor and multisensory cortices compared to sighted subjects (Liu et al., 2007; Yu et al., 2008). In addition, subjects with intensive cross-modal Braille training or early introduction of Braille exhibited improved intrinsic functional connectivity between these brain areas (Liu et al., 2007). The current structural MEMRI and functional connectivity MRI techniques may help uncover the mechanisms of developmental and plastic changes in intrinsic visual and other brain network observed in humans in a systematic manner using well-defined animal models such as the monocular enucleation rodent model in the future (Van Brussel et al., 2011).

To conclude, the results of this study demonstrated MEMRI and RSfcMRI as efficient tools for assessing the structural, physiological and functional neuroarchitecture of the visual brains in vivo, and may possess great potentials for understanding the basic neural forms and functions of the circuitry in the visual system globally and longitudinally. MEMRI allowed

visuotopic brain mapping of retinal, callosal, cortico-subcortical, transsynaptic and intracortical horizontal connections. Layer-specific and topographic visual cortical enhancements could also be differentiated among different routes of Mn^{2+} administration. Loss of visual input upon left eye enucleation appeared to reduce interhemispheric polysynaptic Mn^{2+} transfer but not intra- or inter-hemispheric monosynaptic Mn^{2+} transport after Mn^{2+} injection into right visual cortex. Strengths of resting state functional connectivity appeared to couple with structural connectivity in MEMRI in visual brain network. These structural and functional connectivity MRI techniques may help investigate into the mechanisms of brain connectivity changes during development, plasticity, diseases, pharmacological interventions and genetic modifications in the living visual brains globally and longitudinally in a single setting in future studies.

Acknowledgments

This work was supported by the Hong Kong Research Grant Council (GRF HKU 7837/11M), National Institutes of Health CORE Grant (P30 EY008098) and Cooperative Agreement (UL1 TR000005), BrightFocus Foundation (G2013077), Eye and Ear Foundation of Pittsburgh, and Unrestricted Grant from Research to Prevent Blindness.

References

Abbott CJ, Choe TE, Lusardi TA, Burgoyne CF, Wang L, Fortune B. Imaging axonal transport in the rat visual pathway. Biomed Opt Express. 2013; 4:364–386. [PubMed: 23412846]

Alonso JM, Swadlow HA. Thalamocortical specificity and the synthesis of sensory cortical receptive fields. J Neurophysiol. 2005; 94:26–32. [PubMed: 15985693]

Antonini A, Fagiolini M, Stryker MP. Anatomical correlates of functional plasticity in mouse visual cortex. J Neurosci. 1999; 19:4388–4406. [PubMed: 10341241]

Aoki I, Wu YJ, Silva AC, Lynch RM, Koretsky AP. In vivo detection of neuroarchitecture in the rodent brain using manganese-enhanced MRI. Neuroimage. 2004; 22:1046–1059. [PubMed: 15219577]

Bearer EL, Falzone TL, Zhang X, Biris O, Rasin A, Jacobs RE. Role of neuronal activity and kinesin on tract tracing by manganese-enhanced MRI (MEMRI). Neuroimage. 2007; 37(Suppl 1):S37–46. [PubMed: 17600729]

Bilgen M. Imaging corticospinal tract connectivity in injured rat spinal cord using manganese-enhanced MRI. BMC Med Imaging. 2006; 6:15. [PubMed: 17112375]

Bissig D, Berkowitz BA. Manganese-enhanced MRI of layer-specific activity in the visual cortex from awake and free-moving rats. Neuroimage. 2009; 44:627–635. [PubMed: 19015035]

Bissig D, Berkowitz BA. Same-session functional assessment of rat retina and brain with manganese-enhanced MRI. Neuroimage. 2011; 58:749–760. [PubMed: 21749922]

Canals S, Beyerlein M, Keller AL, Murayama Y, Logothetis NK. Magnetic resonance imaging of cortical connectivity in vivo. Neuroimage. 2008; 40:458–472. [PubMed: 18222710]

Chan KC, Cai KX, Su HX, Hung VK, Cheung MM, Chiu CT, Guo H, Jian Y, Chung SK, Wu WT, Wu EX. Early detection of neurodegeneration in brain ischemia by manganese-enhanced MRI. Conf Proc IEEE Eng Med Biol Soc. 2008a; 2008:3884–3887. [PubMed: 19163561]

Chan KC, Cheng JS, Fan S, Zhou IY, Yang J, Wu EX. In vivo evaluation of retinal and callosal projections in early postnatal development and plasticity using manganese-enhanced MRI and diffusion tensor imaging. Neuroimage. 2011a

Chan KC, Cheng JS, Fan S, Zhou IY, Yang J, Wu EX. In vivo evaluation of retinal and callosal projections in early postnatal development and plasticity using manganese-enhanced MRI and diffusion tensor imaging. Neuroimage. 2012; 59:2274–2283. [PubMed: 21985904]

Chan KC, Cheung MM, Wu EX. In vivo multiparametric magnetic resonance imaging and spectroscopy of rodent visual system. J Integr Neurosci. 2010a; 9:477–508. [PubMed: 21213415]

Chan KC, Fan SJ, Zhou IY, Wu EX. In vivo chromium-enhanced MRI of the retina. Magn Reson Med. 2011b

Chan KC, Fu QL, Guo H, So KF, Wu EX. GD-DTPA enhanced MRI of ocular transport in a rat model of chronic glaucoma. Exp Eye Res. 2008b; 87:334–341. [PubMed: 18639546]

Chan KC, Fu QL, Hui ES, So KF, Wu EX. Evaluation of the retina and optic nerve in a rat model of chronic glaucoma using in vivo manganese-enhanced magnetic resonance imaging. Neuroimage. 2008c; 40:1166–1174. [PubMed: 18272401]

Chan KC, Fu QL, So KF, Wu EX. Evaluation of the visual system in a rat model of chronic glaucoma using manganese-enhanced magnetic resonance imaging. Conf Proc IEEE Eng Med Biol Soc. 2007; 2007:67–70. [PubMed: 18001890]

Chan KC, Khong PL, Lau HF, Cheung PT, Wu EX. Late measures of microstructural alterations in severe neonatal hypoxic-ischemic encephalopathy by MR diffusion tensor imaging. Int J Dev Neurosci. 2009a; 27:607–615. [PubMed: 19505567]

Chan KC, Li J, Kau P, Zhou IY, Cheung MM, So KF, Wu EX. In vivo retinotopic mapping of superior colliculus using manganese-enhanced magnetic resonance imaging. Neuroimage. 2011c; 54:389–395. [PubMed: 20633657]

Chan KC, So KF, Wu EX. Proton magnetic resonance spectroscopy revealed choline reduction in the visual cortex in an experimental model of chronic glaucoma. Exp Eye Res. 2009b; 88:65–70. [PubMed: 18992243]

Chan KC, Xing KK, Cheung MM, Zhou IY, Wu EX. Functional MRI of postnatal visual development in normal and hypoxic-ischemic-injured superior colliculi. Neuroimage. 2010b; 49:2013–2020. [PubMed: 19879366]

Coleman JE, Law K, Bear MF. Anatomical origins of ocular dominance in mouse primary visual cortex. Neuroscience. 2009; 161:561–571. [PubMed: 19327388]

Coogan TA, Burkhalter A. Hierarchical organization of areas in rat visual cortex. J Neurosci. 1993; 13:3749–3772. [PubMed: 7690066]

Cusick CG, Lund RD. The distribution of the callosal projection to the occipital visual cortex in rats and mice. Brain Res. 1981; 214:239–259. [PubMed: 7237170]

Damoiseaux JS, Greicius MD. Greater than the sum of its parts: a review of studies combining structural connectivity and resting-state functional connectivity. Brain Struct Funct. 2009; 213:525–533. [PubMed: 19565262]

Dawson DA, Cha K, Lewis LB, Mendola JD, Shmuel A. Evaluation and calibration of functional network modeling methods based on known anatomical connections. Neuroimage. 2013; 67:331–343. [PubMed: 23153969]

Dreher B, Dehay C, Bullier J. Bihemispheric Collateralization of the Cortical and Subcortical Afferents to the Rat's Visual Cortex. Eur J Neurosci. 1990; 2:317–331. [PubMed: 12106039]

Dreher B, Sefton AJ, Ni SY, Nisbett G. The morphology, number, distribution and central projections of Class I retinal ganglion cells in albino and hooded rats. Brain Behav Evol. 1985; 26:10–48. [PubMed: 3902145]

Failor S, Nguyen V, Darcy DP, Cang J, Wendland MF, Stryker MP, McQuillen PS. Neonatal cerebral hypoxia-ischemia impairs plasticity in rat visual cortex. J Neurosci. 2010; 30:81–92. [PubMed: 20053890]

Greenberg DS, Houweling AR, Kerr JN. Population imaging of ongoing neuronal activity in the visual cortex of awake rats. Nat Neurosci. 2008; 11:749–751. [PubMed: 18552841]

Greicius MD, Supekar K, Menon V, Dougherty RF. Resting-state functional connectivity reflects structural connectivity in the default mode network. Cereb Cortex. 2009; 19:72–78. [PubMed: 18403396]

Harvey AR, Worthington DR. The projection from different visual cortical areas to the rat superior colliculus. J Comp Neurol. 1990; 298:281–292. [PubMed: 2212104]

Hermundstad AM, Bassett DS, Brown KS, Aminoff EM, Clewett D, Freeman S, Frithsen A, Johnson A, Tipper CM, Miller MB, Grafton ST, Carlson JM. Structural foundations of resting-state and task-based functional connectivity in the human brain. Proc Natl Acad Sci U S A. 2013; 110:6169–6174. [PubMed: 23530246]

Honey CJ, Sporns O, Cammoun L, Gigandet X, Thiran JP, Meuli R, Hagmann P. Predicting human resting-state functional connectivity from structural connectivity. Proc Natl Acad Sci U S A. 2009; 106:2035–2040. [PubMed: 19188601]

Hutchison RM, Mirsattari SM, Jones CK, Gati JS, Leung LS. Functional networks in the anesthetized rat brain revealed by independent component analysis of resting-state FMRI. J Neurophysiol. 2010; 103:3398–3406. [PubMed: 20410359]

Innocenti, GM. General Organization of Callosal Connections in the Cerebral Cortex. In: Jones, EG.; Peters, A., editors. Sensory-Motor Areas and Aspects of Cortical Connectivity. Springer; US: 1986. p. 291-353.

Innocenti GM, Aggoun-Zouaoui D, Lehmann P. Cellular aspects of callosal connections and their development. Neuropsychologia. 1995; 33:961–987. [PubMed: 8524456]

Inoue T, Majid T, Pautler RG. Manganese enhanced MRI (MEMRI): neurophysiological applications. Rev Neurosci. 2011; 22:675–694. [PubMed: 22098448]

Jelescu IO, Nargeot R, Le Bihan D, Ciobanu L. Highlighting manganese dynamics in the nervous system of Aplysia californica using MEMRI at ultra-high field. Neuroimage. 2013; 76:264–271. [PubMed: 23523801]

Jurgens CW, Bell KA, McQuiston AR, Guido W. Optogenetic stimulation of the corticothalamic pathway affects relay cells and GABAergic neurons differently in the mouse visual thalamus. PLoS One. 2012; 7:e45717. [PubMed: 23029198]

Karayannis T, Huerta-Ocampo I, Capogna M. GABAergic and pyramidal neurons of deep cortical layers directly receive and differently integrate callosal input. Cereb Cortex. 2007; 17:1213–1226. [PubMed: 16829551]

Keck T, Scheuss V, Jacobsen RI, Wierenga CJ, Eysel UT, Bonhoeffer T, Hubener M. Loss of sensory input causes rapid structural changes of inhibitory neurons in adult mouse visual cortex. Neuron. 2011; 71:869–882. [PubMed: 21903080]

Kondo Y, Takada M, Honda Y, Mizuno N. Bilateral projections of single retinal ganglion cells to the lateral geniculate nuclei and superior colliculi in the albino rat. Brain Res. 1993; 608:204–215. [PubMed: 8495355]

Lau C, Zhang JW, Xing KK, Zhou IY, Cheung MM, Chan KC, Wu EX. BOLD responses in the superior colliculus and lateral geniculate nucleus of the rat viewing an apparent motion stimulus. Neuroimage. 2011a; 58:878–884. [PubMed: 21741483]

Lau C, Zhou IY, Cheung MM, Chan KC, Wu EX. BOLD temporal dynamics of rat superior colliculus and lateral geniculate nucleus following short duration visual stimulation. PLoS One. 2011b; 6:e18914. [PubMed: 21559482]

Liang YX, Cheung SW, Chan KC, Wu EX, Tay DK, Ellis-Behnke RG. CNS regeneration after chronic injury using a self-assembled nanomaterial and MEMRI for real-time in vivo monitoring. Nanomedicine. 2011; 7:351–359. [PubMed: 21185404]

Lin YJ, Koretsky AP. Manganese ion enhances T1-weighted MRI during brain activation: an approach to direct imaging of brain function. Magn Reson Med. 1997; 38:378–388. [PubMed: 9339438]

Lindsey JD, Scadeng M, Dubowitz DJ, Crowston JG, Weinreb RN. Magnetic resonance imaging of the visual system in vivo: transsynaptic illumination of V1 and V2 visual cortex. Neuroimage. 2007; 34:1619–1626. [PubMed: 17204432]

Liu M, Duggan J, Salt TE, Cordeiro MF. Dendritic changes in visual pathways in glaucoma and other neurodegenerative conditions. Exp Eye Res. 2011; 92:244–250. [PubMed: 21310146]

Liu Y, Yu C, Liang M, Li J, Tian L, Zhou Y, Qin W, Li K, Jiang T. Whole brain functional connectivity in the early blind. Brain. 2007; 130:2085–2096. [PubMed: 17533167]

Lund RD, Lund JS. Synaptic adjustment after deafferentation of the superior colliculus of the rat. Science. 1971; 171:804–807. [PubMed: 5549304]

Marshel JH, Garrett ME, Nauhaus I, Callaway EM. Functional specialization of seven mouse visual cortical areas. Neuron. 2011; 72:1040–1054. [PubMed: 22196338]

Martinez-Garcia F, Gonzalez-Hernandez T, Martinez-Millan L. Pyramidal and nonpyramidal callosal cells in the striate cortex of the adult rat. J Comp Neurol. 1994; 350:439–451. [PubMed: 7533799]

Matsuda K, Wang HX, Suo C, McCombe D, Horne MK, Morrison WA, Egan GF. Retrograde axonal tracing using manganese enhanced magnetic resonance imaging. Neuroimage. 2010; 50:366–374. [PubMed: 20074651]

Millecamps S, Julien JP. Axonal transport deficits and neurodegenerative diseases. Nat Rev Neurosci. 2013; 14:161–176. [PubMed: 23361386]

Miller MW, Vogt BA. Direct connections of rat visual cortex with sensory, motor, and association cortices. J Comp Neurol. 1984a; 226:184–202. [PubMed: 6736299]

Miller MW, Vogt BA. Heterotopic and homotopic callosal connections in rat visual cortex. Brain Res. 1984b; 297:75–89. [PubMed: 6722538]

Mizuno H, Hirano T, Tagawa Y. Evidence for activity-dependent cortical wiring: formation of interhemispheric connections in neonatal mouse visual cortex requires projection neuron activity. J Neurosci. 2007; 27:6760–6770. [PubMed: 17581963]

Montero VM. Retinotopy of cortical connections between the striate cortex and extrastriate visual areas in the rat. Exp Brain Res. 1993; 94:1–15. [PubMed: 8335065]

Morch YA, Sandvig I, Olsen O, Donati I, Thuen M, Skjak-Braek G, Haraldseth O, Brekken C. Mn-alginate gels as a novel system for controlled release of Mn2+ in manganese-enhanced MRI. Contrast Media Mol Imaging. 2012; 7:265–275. [PubMed: 22434640]

Olavarria J, Van Sluyters RC. Widespread callosal connections in infragranular visual cortex of the rat. Brain Res. 1983; 279:233–237. [PubMed: 6640342]

Olavarria JF, Laing R, Hiroi R, Lasiene J. Topography and axon arbor architecture in the visual callosal pathway: effects of deafferentation and blockade of N-methyl-D-aspartate receptors. Biol Res. 2008; 41:413–424. [PubMed: 19621122]

Olsen O, Kristoffersen A, Thuen M, Sandvig A, Brekken C, Haraldseth O, Goa PE. Manganese transport in the rat optic nerve evaluated with spatial- and time-resolved magnetic resonance imaging. J Magn Reson Imaging. 2010; 32:551–560. [PubMed: 20815052]

Olsen O, Thuen M, Berry M, Kovalev V, Petrou M, Goa PE, Sandvig A, Haraldseth O, Brekken C. Axon tracing in the adult rat optic nerve and tract after intravitreal injection of MnDPDP using a semiautomatic segmentation technique. J Magn Reson Imaging. 2008; 27:34–42. [PubMed: 18157895]

Pan WJ, Wu G, Li CX, Lin F, Sun J, Lei H. Progressive atrophy in the optic pathway and visual cortex of early blind Chinese adults: A voxel-based morphometry magnetic resonance imaging study. Neuroimage. 2007; 37:212–220. [PubMed: 17560797]

Pautler RG. In vivo, trans-synaptic tract-tracing utilizing manganese-enhanced magnetic resonance imaging (MEMRI). NMR Biomed. 2004; 17:595–601. [PubMed: 15761948]

Pautler RG, Mongeau R, Jacobs RE. In vivo trans-synaptic tract tracing from the murine striatum and amygdala utilizing manganese enhanced MRI (MEMRI). Magn Reson Med. 2003; 50:33–39. [PubMed: 12815676]

Pautler RG, Silva AC, Koretsky AP. In vivo neuronal tract tracing using manganese-enhanced magnetic resonance imaging. Magn Reson Med. 1998; 40:740–748. [PubMed: 9797158]

Pawela CP, Biswal BB, Cho YR, Kao DS, Li R, Jones SR, Schulte ML, Matloub HS, Hudetz AG, Hyde JS. Resting-state functional connectivity of the rat brain. Magn Reson Med. 2008; 59:1021–1029. [PubMed: 18429028]

Paxinos, G.; Watson, C. The rat brain in stereotaxic coordinates. Elsevier Academic Press; 2005.

Paxinos, G.; Watson, C. The rat brain in stereotaxic coordinates. 6. Elsevier; Amsterdam; Boston: 2007a.

Paxinos, G.; Watson, C. The rat brain in stereotaxic coordinates. 6. Academic Press/Elsevier; Amsterdam; Boston: 2007b.

Pietrasanta M, Restani L, Caleo M. The corpus callosum and the visual cortex: plasticity is a game for two. Neural Plast. 2012; 2012:838672. [PubMed: 22792494]

Rothblat LA, Hayes LL. Age-related changes in the distribution of visual callosal neurons following monocular enucleation in the rat. Brain Res. 1982; 246:146–149. [PubMed: 6289971]

Sanderson KJ, Dreher B, Gayer N. Prosencephalic connections of striate and extrastriate areas of rat visual cortex. Exp Brain Res. 1991; 85:324–334. [PubMed: 1716594]

Sherman SM, Guillery RW. The role of the thalamus in the flow of information to the cortex. Philos Trans R Soc Lond B Biol Sci. 2002; 357:1695–1708. [PubMed: 12626004]

Silva AC, Lee JH, Wu CW, Tucciarone J, Pelled G, Aoki I, Koretsky AP. Detection of cortical laminar architecture using manganese-enhanced MRI. J Neurosci Methods. 2008; 167:246–257. [PubMed: 17936913]

Soria G, Wiedermann D, Justicia C, Ramos-Cabrer P, Hoehn M. Reproducible imaging of rat corticothalamic pathway by longitudinal manganese-enhanced MRI (L-MEMRI). Neuroimage. 2008; 41:668–674. [PubMed: 18445533]

Tucciarone J, Chuang KH, Dodd SJ, Silva A, Pelled G, Koretsky AP. Layer specific tracing of corticocortical and thalamocortical connectivity in the rodent using manganese enhanced MRI. Neuroimage. 2009; 44:923–931. [PubMed: 18755280]

Van Brussel L, Gerits A, Arckens L. Evidence for cross-modal plasticity in adult mouse visual cortex following monocular enucleation. Cereb Cortex. 2011; 21:2133–2146. [PubMed: 21310780]

Wang Q, Gao E, Burkhalter A. In vivo transcranial imaging of connections in mouse visual cortex. J Neurosci Methods. 2007; 159:268–276. [PubMed: 16945423]

Wang Q, Gao E, Burkhalter A. Gateways of ventral and dorsal streams in mouse visual cortex. J Neurosci. 2011; 31:1905–1918. [PubMed: 21289200]

Watanabe T, Frahm J, Michaelis T. Functional mapping of neural pathways in rodent brain in vivo using manganese-enhanced three-dimensional magnetic resonance imaging. NMR Biomed. 2004; 17:554–568. [PubMed: 15617054]

Wree A, Angenendt HW, Zilles K. The size of the zone of origin of callosal afferents projecting to the primary visual cortex contralateral to the remaining eye in rats monocularly enucleated at different postnatal ages. Anat Embryol (Berl). 1986; 174:91–96. [PubMed: 3706777]

Yang J, Khong PL, Wang Y, Chu AC, Ho SL, Cheung PT, Wu EX. Manganese-enhanced MRI detection of neurodegeneration in neonatal hypoxic-ischemic cerebral injury. Magn Reson Med. 2008; 59:1329–1339. [PubMed: 18421694]

Yang J, Wu EX. Detection of cortical gray matter lesion in the late phase of mild hypoxic-ischemic injury by manganese-enhanced MRI. Neuroimage. 2008; 39:669–679. [PubMed: 17949999]

Yu C, Liu Y, Li J, Zhou Y, Wang K, Tian L, Qin W, Jiang T, Li K. Altered functional connectivity of primary visual cortex in early blindness. Hum Brain Mapp. 2008; 29:533–543. [PubMed: 17525980]

Yu X, Wadghiri YZ, Sanes DH, Turnbull DH. In vivo auditory brain mapping in mice with Mn-enhanced MRI. Nat Neurosci. 2005; 8:961–968. [PubMed: 15924136]

Zhang J, Ackman JB, Xu HP, Crair MC. Visual map development depends on the temporal pattern of binocular activity in mice. Nat Neurosci. 2012; 15:298–307. [PubMed: 22179110]

Zhou IY, Cheung MM, Lau C, Chan KC, Wu EX. Balanced steady-state free precession fMRI with intravascular susceptibility contrast agent. Magn Reson Med. 2011

Zhou IY, Liang YX, Chan RW, Fan SJ, Gao PP, Cheng JS, So KF, Wu EX. Anatomical/Axonal Basis and Plasticity of Resting-State fMRI Connectivity in an Experimental Model of Corpus Callosum Transection. Proc Intl Soc Mag Reson Med. 2013; 21:32.

Zhou IY, Liang YX, Cheng JS, Chan RW, Chan KC, So KF, Wu EX. Resting-state Functional Connectivity Altered by Complete and Partial Corpus Callosotomy in Rats. Proc Intl Soc Mag Reson Med. 2012; 20:32.

Zoccolan D, Oertelt N, DiCarlo JJ, Cox DD. A rodent model for the study of invariant visual object recognition. Proc Natl Acad Sci U S A. 2009; 106:8748–8753. [PubMed: 19429704]

RESEARCH HIGHLIGHTS

- Manganese-enhanced MRI allowed layer-specific and topographic visual brain mapping
- Retinal, cortico-cortical and cortico-subcortical connections were examined in vivo
- Monocular enucleation to adult rats reduced interhemispheric Mn^{2+} transfer
- Functional connectivity coupled with structural connectivity in the visual brain
- MEMRI and resting-state fMRI can help monitor neurophysiology of visual system

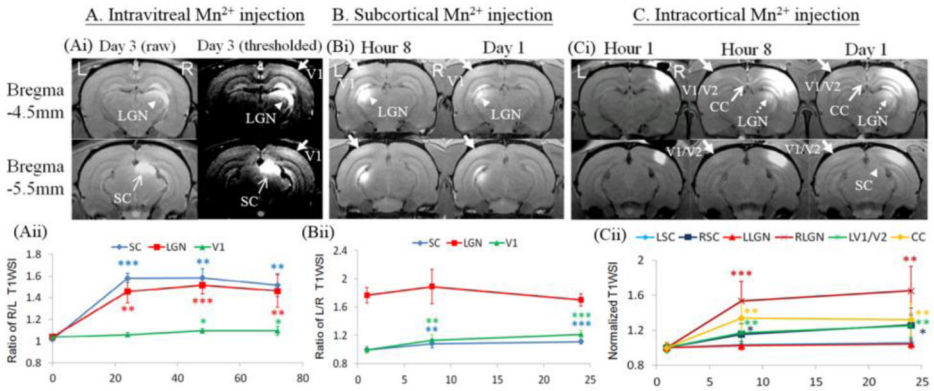

Figure 1.

Differential Mn-enhanced MRI (MEMRI) enhancements in the cortical and subcortical visual brain nuclei via 3 different routes of Mn^{2+} administration using a T1-weighted (T1W) rapid acquisition with relaxation enhancement (RARE) imaging sequence. (A) Intravitreal, fractionated Mn^{2+} injection. (Ai) MEMRI at 3 days after initial Mn^{2+} administration to the left eye. (Aii) Quantitative analyses of T1-weighted (T1W) signal intensity (SI) between right and left superior colliculi (SC), lateral geniculate nuclei (LGN) and primary visual cortex (V1) before, and at 1, 2 and 3 days after initial Mn^{2+} injection; (B) Subcortical, single-dose Mn^{2+} injection. (Bi) MEMRI at 8 hours and 1 day after Mn^{2+} administration to the left LGN. (Bii) Quantitative analyses of T1W SI between left and right SC, LGN and V1 at 1, 8 and 24 hours after subcortical Mn^{2+} injection. (C) Intracortical, single-dose Mn^{2+} injection. (Ci) MEMRI at 1, 8 and 24 hours after Mn^{2+} administration to the right V1/V2 transition zone. (Cii) Quantitative analyses of T1W SI of visual components normalized to Hour 1. Intracortical Mn^{2+} injection appeared to enhance the LGN more locally than intravitreal Mn^{2+} injection. (Two-tailed paired t-tests with 1st time point, *p<0.05; **p<0.01; ***p<0.001)

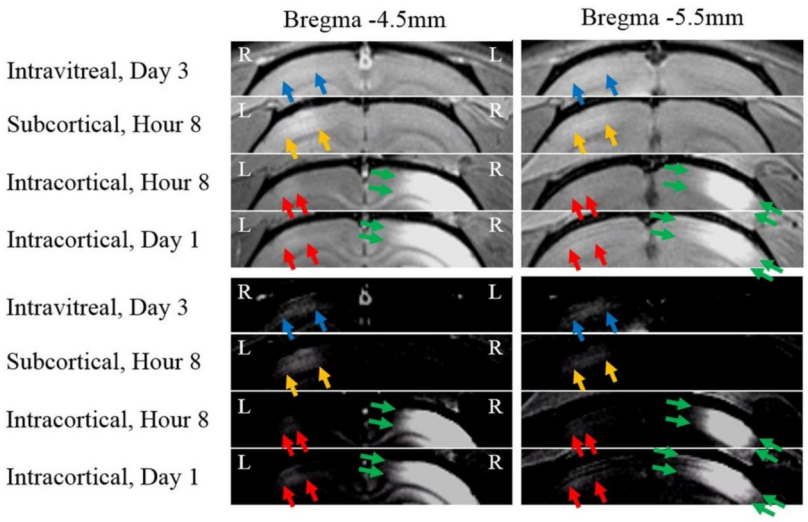

Figure 2.

Topographic visual cortical MEMRI upon 3 different routes of Mn^{2+} administration using the T1W RARE imaging sequence. Zoomed T1W images of the cortical brain regions were shown at Bregma = −4.5mm (left column) and −5.5mm (right column) before (top) and after (bottom) image intensity thresholding for improved contrast. Intravitreal Mn^{2+} injection from contralateral left eye and ipsilateral left subcortical Mn^{2+} injection appeared to enhance the ipsilateral visual cortex more medially (blue and orange arrows) than contralateral right intracortical Mn^{2+} injection (red arrows). Note also the bilaminar intracortical horizontal connections in the ipsilateral right hemisphere (green arrows), which appeared to enhance faster than enhancement by general Mn^{2+} diffusion from injection site.

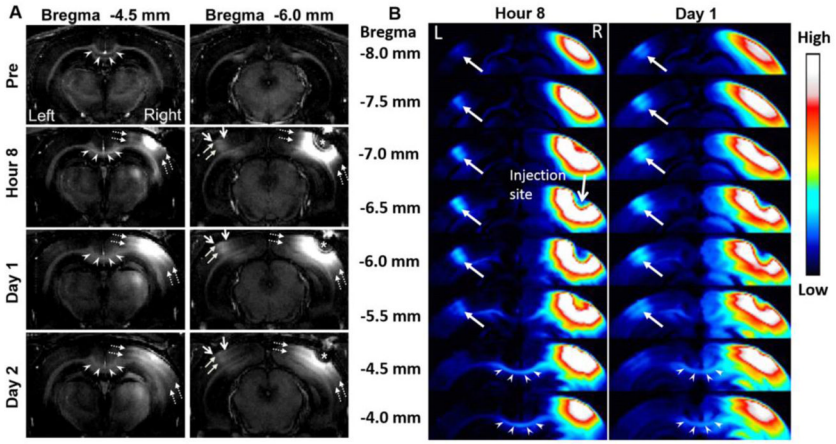

Figure 3.

Spatiotemporal evolution of Mn transport upon intracortical Mn^{2+} injection to visual cortex. (A) Typical modified driven equilibrium Fourier transform (MDEFT) images acquired at 24 hours before (Pre), and at 8 hours, 1 day and 2 days after intracortical Mn^{2+} injection to right visual cortex. Corpus callosum (left column, arrowheads) showed lower signal intensity than surrounding white matter before Mn^{2+} injection, and robust Mn enhancement at 8 hours and later after injection. The contralateral left visual cortex appeared to enhance as a narrow stripe (right column, enclosed by short arrows) with a bi-laminar pattern (right column, long arrows) at 8 hours after Mn^{2+} injection. Such enhancement pattern widened medial-laterally at Day 1 and faded out slightly at Day 2. Bi-laminar Mn enhancement was also observed in the intracortical horizontal connections in the right hemisphere ipsilateral to injection site (dashed arrows). Hypointensity was observed at the injection core (right column, white colored "*") which was likely caused by severe local magnetic field distortion from the highly concentrated Mn^{2+}. (B) Eight consecutive color-coded MDEFT images from Bregma = −4.0mm to −8.0mm, showing prominent transcallosal Mn enhancement in the left hemisphere (closed arrows) and corpus callosum (arrowheads) 8 hours (left column) and 1 day (right column) after intracortical Mn^{2+} injection into right visual cortex (open arrow).

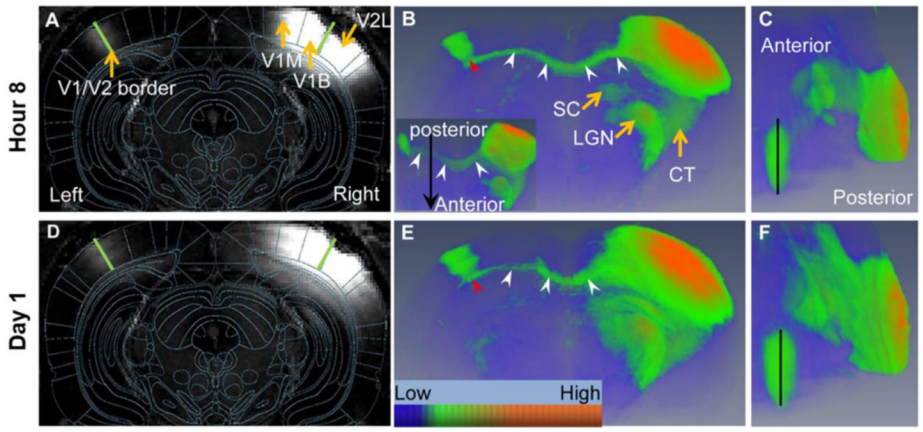

Figure 4.

MDEFT images overlaid on the standard rat brain atlas at Bregma −6.0 mm (A, D), and reconstructed 3D MDEFT color images showing the coronal view of the transcallosal Mn^{2+} transport pathway via the splenium of corpus callosum (B, E; white arrowheads; looking from posterior to anterior directions) and the spread of Mn^{2+} enhancement from 8 hours (top row) to 1 day (bottom row) after intracortical Mn^{2+} injection in both coronal (B, E) and sagittal views (C, F; looking from left to right directions). Green lines in panels A and D represent the V1/V2 border. Red arrowheads in panels B and D, and black lines in panels C and F show the medial-lateral spread of the contralateral hemisphere enhancement over time. The inset in panel B illustrates the Mn^{2+} transport pathway viewing from the cranial base in ventral to dorsal directions. V1M: monocular primary visual cortex; V1B: binocular primary visual cortex; V2L: lateral secondary visual cortex; LGN: lateral geniculate nucleus; SC: superior colliculus; CT: cortico-thalamic connections.

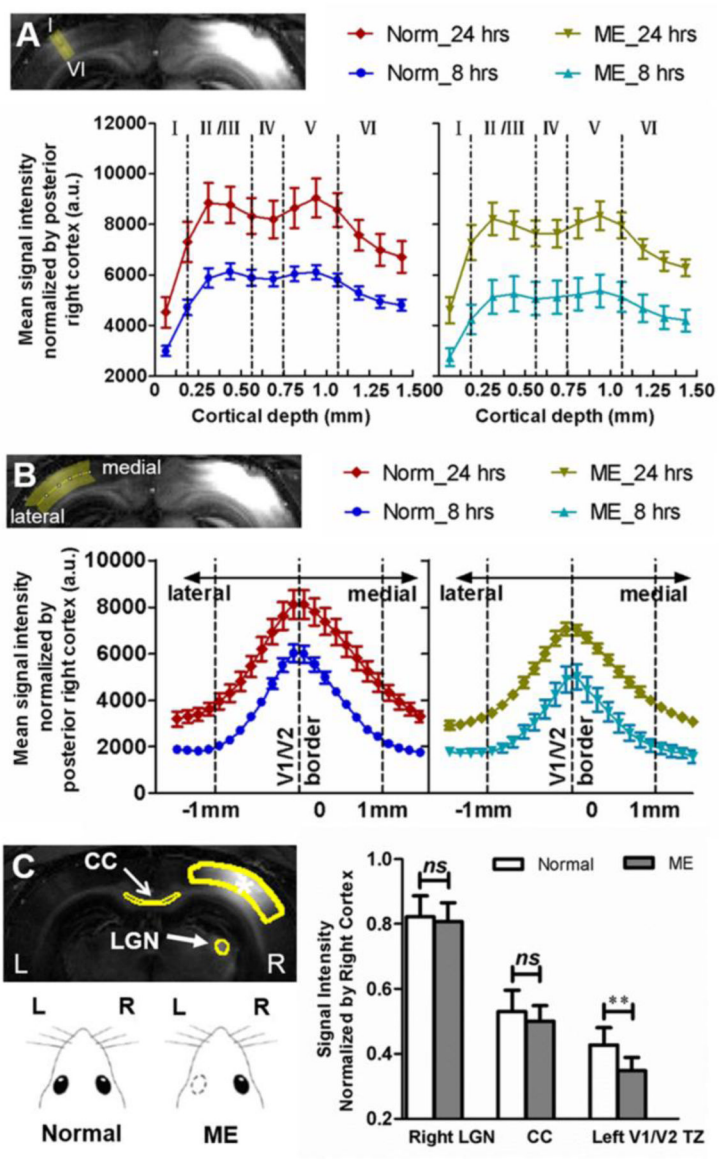

Figure 5.

Quantitative evaluation of the spatiotemporal distributions of transcallosal Mn transport (A–C) and corticothalamic Mn transport (C) at 8 (A and B) and 24 hours (A–C) after intracortical Mn^{2+} injection to right visual cortex. (A) Layer-specific Mn enhancement profile across cortical depth at the left V1/V2 transition zone (yellow in inset), and (B) Mn enhancement profile along medial-lateral direction in the left V1/V2 transition zone (yellow in inset) in normal rats (left) and visually deprived rats after monocular enucleation (ME) of left eye (right). In both normal and ME rats, Mn enhancement appeared to peak at layers II, III and V near the left V1/V2 border in (A) at both 8 and 24 hours after Mn^{2+} injection ($p<0.05$ between layers). Medial-laterally, Mn enhancement was confined within 1 mm from left V1/V2 border at 8 hours and spread out thereafter (B) ($p<0.01$ between 0 and 1mm from left V1/V2 border; $p<0.05$ between Hour 8 and Hour 24). A global decrease in Mn^{2+} enhancement at the left V1/V2 transition zone was also observed both across cortical depth and along medial-lateral directions in the ME rats compared to normal rats. No statistical difference was observed in corpus callosum and LGN enhancement between normal and ME

rats, while the left V1/V2 transition zone was significantly less enhanced in the latter group by about 18.5% on average (C) (**$p<0.01$). Data are shown as mean ± standard error of mean.

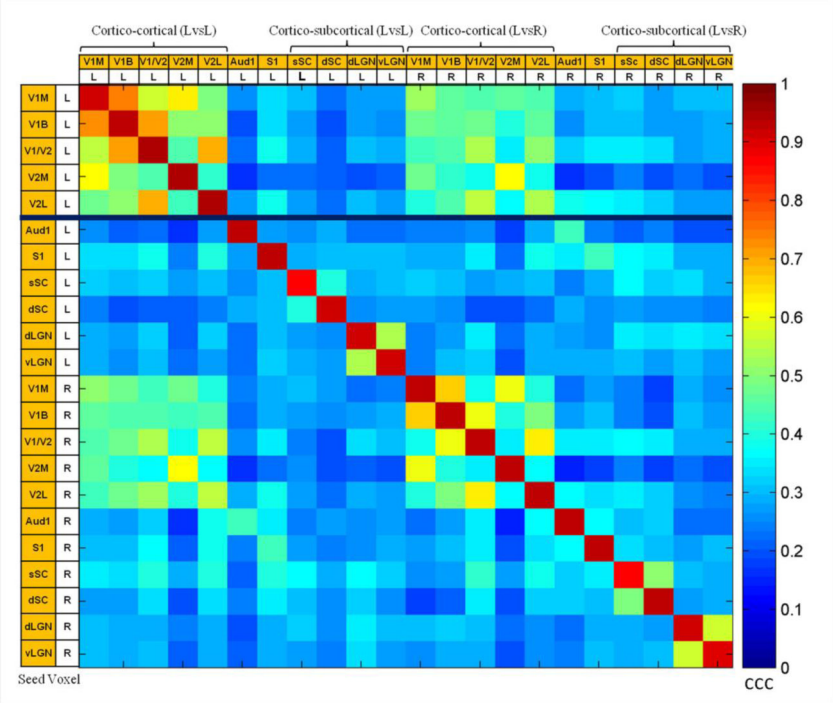

Figure 6.

Resting-state functional connectivity MRI of visual brain network. As seen in the cross-correlation coefficient (ccc) map of spontaneous low frequency fluctuations between different brain regions along horizontal and vertical axes, intrahemispheric cortical connectivity [e.g. corticocortical (LvsL) network above bold horizontal line] ($p<0.05$) appeared to be in general stronger than interhemispheric cortical connectivity [e.g. corticocortical (LvsR) network above bold horizontal line], whereas corticocortical connectivity appeared to be in general stronger than cortico-subcortical connectivity intra- and inter-hemispherically ($p<0.05$). Comparing among interhemispheric cortico-cortical network, V1/V2 transition zone in one hemisphere possessed the highest mean correlation coefficient with contralateral V1/V2 transition zone relative to other cortical nuclei measured in the contralateral hemisphere. This appeared to be consistent with MEMRI observations in previous figures, showing more direct transcallosal anatomical connections to contralateral V1/V2 transition zone upon intracortical Mn^{2+} injection to ipsilateral V1/V2 transition zone. Comparing among cortico-subcortical network, those with more direct anatomical visual connections traced by MEMRI [(e.g. visual cortex vs superficial layers of superior colliculus (sSC)] also showed stronger functional connectivity than the less direct anatomical network [(e.g. visual cortex vs deep layers of superior colliculus (dSC)] ($p<0.05$). Primary somatosensory cortex (S1) appeared to have a stronger correlation with the visual brain network compared to primary auditory cortex (Aud1) in the same hemisphere ($p<0.05$). (V1M: monocular primary visual cortex; V1B: binocular primary visual cortex; V1/V2: V1/V2 transition zone; V2M: medial secondary visual cortex; V2L: lateral secondary visual cortex)

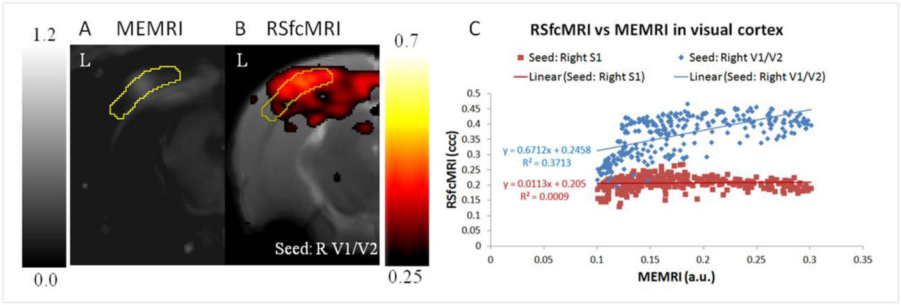

Figure 7.

(A) Mean manganese-enhanced T1-weighted MR image (MEMRI) of left hemisphere at 1 day after Mn injection to right visual cortex, and (B) the corresponding cross-correlation coefficient (ccc) color map of resting-state functional connectivity MRI (RSfcMRI) overlaid on the T2-weighted image upon seed voxel placement in the right V1/V2 transition zone. (C) Scatter plots of resting-state functional connectivity against normalized manganese-enhanced T1-weighted signal intensities in the left visual cortex covered by the same yellow regions-of-interest in (A) and (B). Voxel-by-voxel comparisons between RSfcMRI and MEMRI in the left visual cortex indicated the strong positive correlation between structural and functional connectivity using right V1/V2 but not right S1 as the seed voxel.